Fast electrons from electron-ion collisions in strong laser fields

H.-J. Kull[a)]
Institute of Theoretical Physics A, RWTH Aachen University, Templergraben 55, 52056 Aachen, Germany

V. T. Tikhonchuk[b)]
Centre Lasers Intenses et Applications, UMR 5107 CNRS - Université Bordeaux 1 - CEA, Université Bordeaux 1, 33405 Talence Cedex, France

(Received 6 July 2004; accepted 31 March 2005; published online 26 May 2005)

Electron-ion collisions in the presence of a strong laser field lead to a distribution of fast electrons with maximum energy $E_{max}=(k_0+2v_0)^2/2$(a.u.), where k_0 is the impact and v_0 the quiver velocity of the electron. The energy spectrum is calculated by two approaches: (1) The time-dependent Schrödinger equation is numerically solved for wave packet scattering from a one-dimensional softcore Coulomb potential. Multiphoton energy spectra are obtained demonstrating a separation of the energy spectrum into an exponential distribution for transmission and a plateau distribution for reflection. (2) The energy spectrum is analytically calculated in the framework of classical instantaneous Coulomb collisions with random impact parameters and random phases of the laser field. An exact solution for the energy spectrum is obtained from which the fraction of fast electrons in the plateau region can be estimated. © *2005 American Institute of Physics*. [DOI: 10.1063/1.1924457]

I. INTRODUCTION

Scattering of electrons on ions in the presence of strong laser fields plays an important role for above threshold ionization (ATI) of atoms and inverse bremsstrahlung absorption (IBA) in plasmas. The main differences between ATI and IBA arise from different initial conditions. In ATI, an atom is first ionized and then the electron returns to the ion with relatively small velocities and impact parameters. One of the prominent features is a plateau in the energy spectrum as a result of rescattering after ionization.[1–6] In IBA a free electron is scattered with relatively large velocities and impact parameters. Multiphoton transitions in strong fields lead to a nonlinear electrical conductivity relationship that has been the topic of various theoretical approaches.[7–14]

In this work, we wish to draw attention to a fast-electron population that can be generated by collisions in strong laser fields at relatively small impact parameters, typically less than the atomic unit, and at relatively large impact velocities, typically a few times the quiver velocity. This parameter regime is apparently not well covered by ATI where the characteristic impact velocities are smaller or by IBA where the characteristic impact parameters are larger. It is our purpose to discuss the energy distribution in this intermediate parameter regime and to estimate the fraction of fast electrons produced. A detailed knowledge of the fast electron distribution is of particular importance for further atomic processes, e.g., inner-shell ionization, in high intensity laser plasma experiments.[15] It may also be useful as an input to plasma simulations where large-angle collisions are commonly neglected. Furthermore future experiments with electron and laser beams could lead to a direct verification of these predictions.

The basic mechanism of energy transfer in a strong field can be simply understood in terms of an oscillating mirror model. Assume an electron, oscillating in a laser field, is normally incident on a plane surface and is instantaneously reflected there. In a coordinate frame, moving with the quiver velocity, this process can be viewed as reflection by an oscillating mirror. The corresponding energy transfer is given below by Eq. (34). It can be measured after the electron has left the laser field.

A complete solution of the corresponding quantum-mechanical scattering problem for electron-ion collisions would be quite demanding. We therefore have chosen a two-step analysis: First, the oscillating mirror model is treated quantum mechanically for a one-dimensional (1D) softcore Coulomb potential. Results from these quantum calculations are found in general accordance with a simple model of classical instantaneous collisions. Therefore, in the second step, the classical 1D model is generalized to a 3D Coulomb problem and the energy distribution of the scattered electrons is calculated in this framework.

The 1D scattering problem can be numerically solved in the framework of the time-dependent Schrödinger equation (TDSE). A method of wave packet scattering is introduced to calculate the energy spectra. The softcore Coulomb potential accounts for different degrees of reflection and transmission. This model allows one to calculate multiphoton energy spectra and to study the asymmetries for forward and backward scattered particles that are quite specific for the present energy transfer mechanism. With increasing impact velocity, it is found that there is a clear separation between an exponential distribution in the forward and a plateau distribution in the backward direction. This asymmetry has not yet been observed in ATI experiments, most likely because the symmetry of the atomic initial state makes it difficult to control the impact direction. Asymmetries in ATI have recently been

[a)]Electronic mail: kull@ilt.fhg.de
[b)]Electronic mail: tikhon@celia.u-bordeaux1.fr

observed for few-cycle pulses, but at present they refer to total counting rates only.[16]

In the past, 1D models have been widely used for studying strong field ionization,[17–19] detachment,[20,21] capture,[22,23] stabilization,[24,25] and scattering.[26] In the present work the short distance cutoff of the softcore potential is crucial for the formation of the scattering plateau. Reflection from a 1D attractive potential is a quantum feature that can only be observed if the potential parameters violate to some extent the quasiclassical approximation. High reflectivities require a cutoff well below 1 a.u. In this respect, the present work differs from most previous numerical studies. It also extends the scope of other scattering studies being addressed to the ATI regime[22,23,26] or to atoms with short-range potentials.[27]

In the 3D problem, we consider binary collisions of electrons with fixed ions in the presence of a laser field. Potential scattering in strong fields has been treated in early work by Bunkin and Fedorov[28] and by Kroll and Watson.[29] The quantum-mechanical treatment based on the Born approximation leads to similar results as the classical treatment of instantaneous collisions. The basic result in these works is the quantum-mechanical cross section for multiphoton scattering, which can be viewed as a discrete energy distribution. In the classical limit a continuous average distribution is obtained. However, these distributions still depend on the scattering angle and angle-integrated total distributions have only been given in a few cases.[28] A later review of the subject deals primarily with total energy absorption rates without addressing the issue of energy distributions.[30]

The classical model of instantaneous collisions is based on the assumption that the duration of collisions is much shorter than the laser period. During the collision the momentum change by the laser field is neglected and scattering is described by the Coulomb potential only. The laser field enters as a parameter through the impact velocity. It is noted that the classical Coulomb cross section is exact in quantum theory. Therefore the classical treatment should be no serious limitation as long as the approximation of instantaneous collisions is satisfied. We briefly review the model of instantaneous collisions and then derive the energy spectrum in this framework. For definiteness the geometry of parallel launch is chosen, where the electrons are incident parallel to the polarization direction of the laser field. Such conditions can be met, e.g., in experiments with mutually perpendicular laser and electron beams, overlapping within the plasma volume. Expressing the Coulomb-scattering rate as a function of the energy transfer and integrating over random collision phases, the energy distribution can be analytically calculated. The total energy distribution for instantaneous Coulomb collisions with random impact parameters and collision phases represents one of the major results of this work.

The paper is organized as follows. The 1D model and the method of wave packet scattering are introduced in Sec. II. It is explained how energy spectra with the required energy resolution can be calculated from the asymptotic wave function after the interaction. In Sec. III scattering is studied without laser field. The present time-dependent method is compared with time-independent stationary solutions and the reflection coefficient for the softcore Coulomb potential is discussed. The numerical results of the scattering problem with laser field are presented in Sec. IV. These include energy spectra for different initial energies and corresponding wave functions. The energy distributions are analytically explained in the context of the classical instantaneous collision model in Sec. V. This model is extended to 3D Coulomb collisions. The derivation of the energy spectrum requires a specific integration over collision phases for a given energy transfer that is discussed in the Appendix.

II. SCATTERING MODEL

As a model of electron-ion collisions, we consider scattering from a 1D model potential. Basically, the model describes normal incidence of a stream of electrons on a plane layer of ions. The polarization direction of the laser field is assumed parallel to the launch direction. Despite the obvious simplifications in this model, the energy spectrum of backscattered electrons can be quite well understood in this framework and complete numerical solutions of the TDSE can be gained. Extensions to real Coulomb collisions will be discussed in Sec. V.

As a model potential, we choose a softcore Coulomb potential with charge state Z and cutoff distance ϵ,

$$V(x) = -\frac{Z}{\sqrt{x^2+\epsilon^2}}, \tag{1}$$

where all quantities are expressed in atomic units ($m=-e=\hbar=1$, m is the electronic mass, e is the electronic charge, $\hbar$ is Planck's constant). The dependence of the reflection coefficient on the parameters Z and ϵ will be discussed in detail in Sec. III. In most numerical calculations $Z=1$ and $\epsilon=0.1$ have been chosen. The laser field is described in the dipole approximation as a time-dependent electric field

$$\varepsilon(t) = \varepsilon_0 \sin(\omega_0 t), \tag{2}$$

with amplitude ε_0 and frequency ω_0. Specifically, we set $\varepsilon_0=0.2$ and $\omega_0=0.2$. These parameters correspond to an intensity of 1.4×10^{15} W/cm^2 and a wavelength of 0.23 μm, respectively. The quiver velocity is $v_0=\varepsilon_0/\omega_0=1.0$ and the ponderomotive potential $U_p=v_0^2/4=0.25$. It is noted that the typical energy of backscattered electrons, $(2v_0)^2/2=8U_p=10\omega_0$, is much larger than the photon energy. Depending on the incident particle energy, typical energy spectra extend up to 20–100 photon orders for these parameters.

It is convenient to describe the interaction with the laser field in the Kramers–Henneberger (KH) coordinate frame, whose origin is displaced with respect to the laboratory frame by the quiver amplitude,

$$\xi(t) = \xi_0 \sin(\omega_0 t), \quad \xi_0 = \varepsilon_0/\omega_0^2. \tag{3}$$

In this frame, the quiver motion $\xi(t)$ of the electron in the laser field is removed at the expense that the electron is now scattered by an oscillating potential $V(x+\xi)$. Assuming that the laser pulse is switched on and off adiabatically in time, the asymptotic electron velocities calculated in the KH frame will be equal to the velocities measured in the laboratory frame outside of the laser pulse. For this reason the KH frame is particularly well suited for the calculation of the

energy spectra. The TDSE in the KH frame has the well-known form,

$$i\partial_t\psi(x,t) = \left[-\tfrac{1}{2}\partial_x^2 + V(x+\xi)\right]\psi(x,t). \tag{4}$$

In this work, Eq. (4) has been solved numerically by the Crank–Nicholson method.[31,32] A large spatial grid, $|x| < 2500$–3000, is used to obtain an accurate representation of the scattered wave function in the asymptotic regions without boundary effects. The calculations are performed over an interaction time of 16 laser periods. The spatial grid has the step width $\Delta x = 0.1$ and the time step is taken as $\Delta t = 0.03$. Decreasing either Δx or Δt did not lead to significant changes of the results presented.

The time-dependent scattering problem has been studied by the method of wave packet scattering. In the initial state, a wave packet is launched from the left asymptotic region toward the scattering center. Its time evolution is followed up to a final state with well separated transmitted and reflected wave packets. Subsequently the energy spectra of the transmitted and reflected wave packets are analyzed in the asymptotic regions. The initial wave packet is chosen as a plane wave with a Gaussian envelope,

$$\psi_0(x) = e^{ik_0x}e^{-(x-x_0)^2/d^2}. \tag{5}$$

For initial velocities k_0 in the range between 1 and 5, the initial position x_0 and the width d are chosen as

$$x_0 = -\tfrac{1}{2}k_0\tau, \quad \tau = 16\frac{2\pi}{\omega_0}, \quad d = \frac{2}{5}|x_0|. \tag{6}$$

Within the computation time τ, a free wave packet moves the distance $2|x_0|$ from $-|x_0|$ to $+|x_0|$. Specifically, $\tau \approx 500$, $|x_0| \approx 250$, and $d \approx 100$ for $k_0 = 1$. The width of the Gaussian increases in the course of time by the factor $\sqrt{1+4t^2/d^4}$. However, for small de Broglie wavelengths with $k_0 d \gg 10$, this broadening of the packet is still small at the final time τ,

$$\frac{4\tau^2}{d^4} = 16\frac{x_0^2}{k_0^2 d^4} = \left(\frac{10}{k_0 d}\right)^2 \ll 1. \tag{7}$$

In choosing the width of the Gaussian, it has to be optimized to ensure a proper localization of the wave function both in real space and in momentum space. This leads to the condition

$$k/\omega_0 \ll d \ll |x_0|. \tag{8}$$

Evidently, the width has to be smaller than the distance $|x_0|$ from the scattering potential. On the other hand, d has to be large enough such that a spectral line can be well resolved up to one photon energy. In momentum space the wave packet has a width $\Delta k \approx 1/d$. For a free particle, the corresponding energy width is $\Delta E = k\Delta k$ and from the requirement $\Delta E \ll \omega_0$ there follows the criterion $d \gg k/\omega_0$. The minimum width is of the order of the distance traveled by the packet in one laser period. For the given parameters different photon orders can be very well resolved and only substructures within the lines may be smoothed out.

The energy spectra of the asymptotic wave packets are analyzed in the following manner. The asymptotic regions are defined as $-x_b < x < -x_a$ to the left side and $x_a < x < x_b$ to the right side of the potential, where $x_a = 10 + \xi_0 = 15$ is taken as the inner and $x_b = 2500$ as the outer boundary. The results do not depend in a sensitive way on the precise position of these boundaries. Spatial Fourier transforms ψ_k^l and ψ_k^r of the wave function are calculated for the left and right intervals,

$$\psi_k^l = \int_{-x_b}^{-x_a} dx\ \psi e^{-ikx}, \quad k<0,$$

$$\psi_k^r = \int_{x_a}^{x_b} dx\ \psi e^{-ikx}, \quad k>0,$$

respectively. Being only interested in outgoing waves, we restrict attention on the left to negative and on the right to positive wave numbers. The energy is formally taken negative for $k<0$ and positive for $k>0$,

$$E = \tfrac{1}{2}k^2[-\Theta(-k) + \Theta(k)], \tag{9}$$

and the energy spectrum is defined by

$$P(E) = \frac{1}{2\pi N|k|}[\Theta(-k)|\psi_k^l|^2 + \Theta(k)|\psi_k^r|^2], \tag{10}$$

where $\Theta(x)$ denotes the Θ function and $N = \sqrt{\pi/2d}$ is the norm of the wave function. The energy spectrum integrated over positive and negative energies is normalized to unity,

$$\int_{-\infty}^{+\infty} dE\ P(E) = \int_{-\infty}^{0} \frac{dk}{2\pi N}|\psi_k^l|^2 + \int_0^{+\infty} \frac{dk}{2\pi N}|\psi_k^r|^2 = 1. \tag{11}$$

III. SCATTERING WITHOUT LASER FIELD

In the absence of the laser field, the wave packet is scattered elastically by the static softcore Coulomb potential. This problem is considered here, first, as a reference for the case with laser field, second, to validate the time-dependent wave packet method against stationary scattering solutions, and third, to calculate the reflection coefficient as a function of the present parameters. The reflection coefficient is a key quantity to characterize the fraction of fast electrons and it turns out that the field-free reflection coefficient often provides a useful first estimate.

The stationary scattering solutions can be obtained from the time-independent Schrödinger equation

$$-\tfrac{1}{2}\partial_x^2\psi + V(x)\psi = E\psi \tag{12}$$

by choosing an energy $E = k_0^2/2$ and the boundary condition $\psi \to e^{ik_0x}$ for the transmitted wave at $x \to +\infty$. For convenience, the amplitude of the transmitted wave is normalized equal to unity. The second-order differential equation has been transformed to a system of two first-order equations and integrated backwards, from the right-hand side to the left-hand side, by a fourth-order Runge–Kutta method.

As an example, Fig. 1 shows a comparison of scattering solutions for $k_0 = 1$. It represents (a) the stationary solution according to Eq. (12), (b) the time-dependent solution for a Gaussian wave packet after 8 periods when its maximum has reached the center, and (c) a time-dependent solution after 16 periods that corresponds to a plane wave initial condition, $\psi_0 = e^{ik_0x}$. On the left side, the superposition of the incident

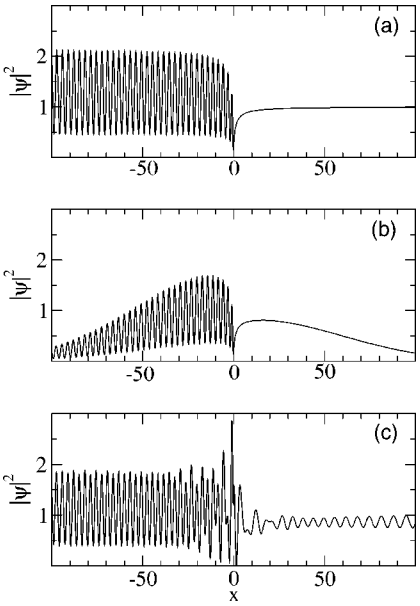

FIG. 1. Scattering of a plane wave with initial velocity $k_0=1$ for $\varepsilon=0$. (a) Time-independent stationary solution, (b) time-dependent solution for a Gaussian wave packet after 8 periods, (c) time-dependent solution for plane wave initial conditions after 16 periods.

and reflected waves leads to a standing wave with wavelength $2\pi/2k_0=\pi$. On the right side, only the amplitude of the transmitted wave should be present. The wave packet solution closely resembles the stationary solution with a Gaussian envelope. Furthermore it very well satisfies the outgoing wave boundary condition for the transmitted wave. With the plane wave initial condition in (c) the stationary state cannot be approached with comparable accuracy.

Returning now to the evolution of the Gaussian wave packet, its wave function and its energy spectrum after 16 periods are shown in Fig. 2. The wave packet has well separated into a transmitted and a reflected one. The maxima are close to the positions ± 250, corresponding to free propagation. The probability within the interaction region is only of the order of 10^{-6}. The energy spectrum shows corresponding peaks at the energies $E=\pm 0.5k_0^2=\pm 0.5$ of the incident and reflected waves. The peaks are very well resolved with respect to the photon energy $\omega_0=0.2$ and they can be clearly identified for more than six orders of magnitude.

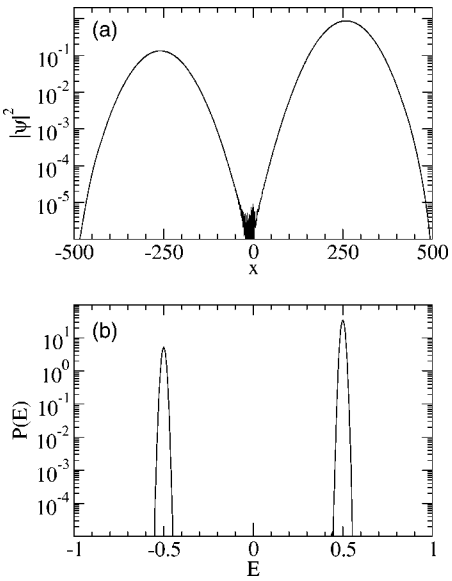

FIG. 2. Scattering of a Gaussian wave packet with velocity $k_0=1$ without laser field ($\varepsilon=0$). (a) Probability density $|\psi|^2$ and (b) energy spectrum $P(E)$ after 16 periods.

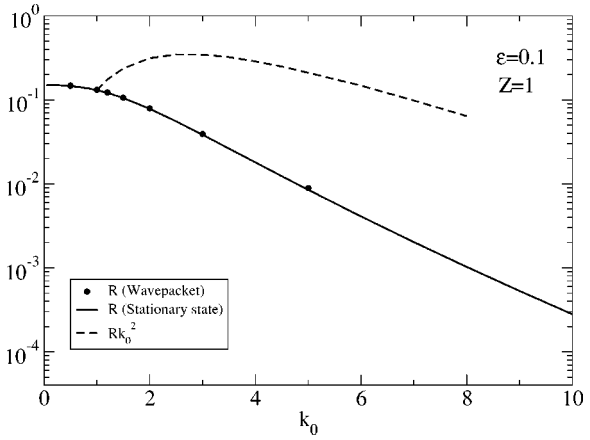

FIG. 3. Reflection coefficient R for the softcore Coulomb potential ($\epsilon=0.1, Z=1$) as a function of the initial velocity k_0. (Solid, time-independent calculation; dots, time-dependent wave packet calculation; dashed, Rk_0^2.)

Finally, we discuss the reflection coefficient as a function of the parameters k_0, Z, and ϵ. The reflection coefficient of the stationary solution is defined in terms of the amplitudes of the incident and reflected waves,

$$C_{i,r}=\frac{1}{2ik}(\partial_x\psi \pm ik\psi), \quad k=\sqrt{k_0^2-2V}, \tag{13}$$

respectively, as

$$R=\left|\frac{C_r}{C_i}\right|^2=\left|\frac{\partial_x\psi-ik\psi}{\partial_x\psi+ik\psi}\right|^2. \tag{14}$$

Here $k(x)$ denotes the local wave number. The reflection coefficient of the nonstationary wave packet solution is more conveniently calculated by the probability of finding the particle in the left asymptotic region at the final time of the calculation,

$$R=\frac{1}{N}\int_{-x_b}^{-x_a} dx|\psi|^2. \tag{15}$$

Assuming that the reflected flux is a constant fraction R of the incident flux at the inner boundary $-x_a$ and that the initial wave packet has finally completely passed this boundary, these definitions should be equivalent. In Fig. 3 both reflection coefficients are represented as a function of the incident velocity k_0 for $Z=1$ and $\epsilon=0.1$. The results of both computational methods are in excellent agreement. The reflection coefficient approaches a finite value for slow particles and decreases exponentially with increasing velocities.

To relate the results of the 1D model to 3D Coulomb collisions one may compare the wave functions of both scattering solutions on the x axis near the scattering center. As-

ymptotically, the solutions are superpositions of incoming and scattered waves. However, in 3D the amplitude of the scattered wave decreases with distance in contrast to the constant amplitude in 1D. Therefore, one has to choose a physically meaningful reference point for the definition and comparison of reflection coefficients. Since the asymptotic representation of the wave function becomes valid for $k_0|x| \gg 1$, we have chosen the reference point at $x_R=-1/k_0$, which scales with the de Broglie wavelength of the incident particle. Evaluating the known asymptotic solution of the Coulomb problem at x_R, the corresponding reflection coefficient is found to be

$$R_C = \sigma_C^B k_0^2 = \frac{1}{4k_0^2}, \quad \sigma_C^B = \frac{1}{4k_0^4}, \tag{16}$$

where σ_C^B is the Coulomb cross section for backscattering. Since $R_C k_0^2 = 0.25$ is constant, we have evaluated this parameter for the 1D model (Fig. 3). There is a reasonably good agreement, $Rk_0^2 = 0.25 \pm 0.1$, in the range of velocities $1.5 < k_0 < 5$. This comparison shows that the 1D model with $\epsilon = 0.1$ yields about the same energy scaling of the reflection coefficient as 3D Coulomb collisions within the given range of impact velocities. For larger velocities, $k_0 \gtrsim 5$, the characteristic impact parameters become smaller than the present cutoff distance $\epsilon = 0.1$ and the softcore potential then appreciably differs from the Coulomb field. For instance, it is noted that the impact parameter for 90° deflections, $b_\perp = 1/k_0^2$, is 0.04 at $k_0 = 5$.

A simple transformation of parameters shows that the reflection coefficient is actually a function of two parameters only. Setting $u = x/\epsilon$, $p = k_0\epsilon$, and $q = Z\epsilon$ in Eq. (12) yields

$$\partial_u^2 \psi + \left[p^2 + \frac{q}{\sqrt{u^2+1}} \right] \psi = 0. \tag{17}$$

The reflection coefficient can therefore be expressed as a function $R = R(p,q)$. The regime of slow particles can be defined by the condition $p \ll 1$ for $q = O(1)$. In this regime the initial velocity becomes negligible and the reflection coefficient depends on the potential parameter q only. This conclusion is illustrated by the numerical evaluation shown in Fig. 4. For sufficiently large Z, the influence of the initial velocity becomes negligible for fixed q and the reflection coefficient approaches a unique asymptote $R = R(q)$ in all cases. On this asymptote an increase of Z decreases reflectivity. This apparently counterintuitive result is explained by the fact that a stronger potential leads to higher velocities and consequently to a shorter de Broglie wavelength, favoring the transmission of the particle.

Reflection by a 1D attracting potential is a purely quantum-mechanical feature. Obviously, a classical particle will not reach a turning point where its velocity goes to zero. A criterion for the reflection efficiency of the potential may be gained by considering its violation of the semiclassical WKB approximation. Within the WKB approximation a wave can propagate without significant reflection with the local wave number $k(x)$ given in Eq. (13). The WKB approximation applies to weak inhomogeneities satisfying

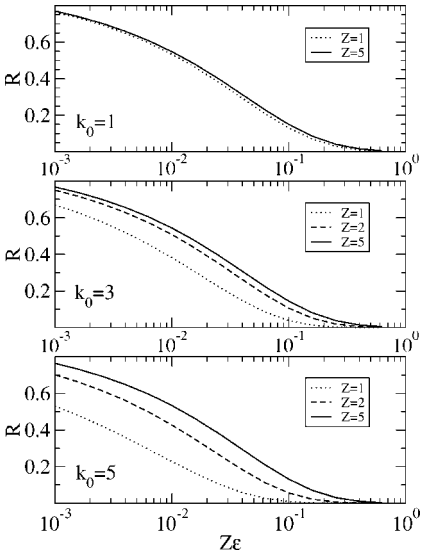

FIG. 4. Reflection coefficient R for the softcore Coulomb potential as a function of the parameters Z and ϵ for three different initial velocities k_0. For large Z all curves approach a unique asymptote $R = R(Z\epsilon)$, depending on $Z\epsilon$ only.

$$\frac{\partial_x k}{k} \ll k. \tag{18}$$

Restricting attention to slow particles with $k_0^2 \ll k^2$, this condition can be rewritten as a criterion for the potential,

$$|\partial_x V| \ll (2|V|)^{3/2}. \tag{19}$$

Using the potential (1), one finds

$$\frac{x}{(x^2+\epsilon^2)^{3/4}} \ll \sqrt{8Z}. \tag{20}$$

The left-hand side assumes its maximum value for $x = \sqrt{2}\epsilon$, yielding

$$\sqrt{Z\epsilon} \gg \frac{1}{2}\frac{1}{3^{3/4}}. \tag{21}$$

Conversely, the criterion for efficient reflection of the softcore Coulomb potential may be expressed in the simple form

$$Z\epsilon \ll 1. \tag{22}$$

We have also studied reflection from a $V = -1/\cosh^2(x/\epsilon)$ potential and therefore arrived at an analogous condition $\epsilon \ll 1$ for reflection. This explains the absence of a scattering plateau in the energy spectra of the model potential $V = -1/\cosh^2(x)$ used previously.[19]

IV. SCATTERING WITH LASER FIELD

In the presence of both the laser field and the scattering potential an electron can gain or lose energy. If electrons with initial energy E_i absorb or emit an integer number n of photons in a free-free transition, the spectrum will consist of a series of peaks at the energies

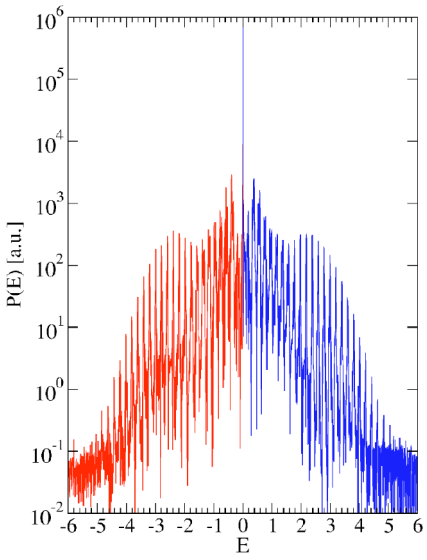

FIG. 5. Energy spectrum for scattering with zero initial momentum. One can observe spatially symmetric ATI-type scattering plateaus on both sides of the scattering center.

$$E_n = E_i + n\omega_0. \tag{23}$$

Similar spectra are observed in above threshold ionization of atoms in strong laser fields. For an atom with ionization potential I_p in a field with ponderomotive potential U_p the final energy is given by

$$E_n = -(I_p + U_p) + n\omega_0. \tag{24}$$

The structure of ATI spectra has been widely studied in the past.[21,22] In this work, we consider the related scattering problem and discuss the dependence of the energy spectrum on the initial energy of the electrons.

To demonstrate more explicitly the relationship between scattering and ionization, we first consider an initial state

$$\psi_0 = 1. \tag{25}$$

It can be viewed as the limit of a Gaussian wave packet with zero momentum, $k_0=0$, and infinite width, $d\to\infty$. It is noted that the classical analog of the zero momentum state is an ensemble of electrons distributed uniformly in the potential with zero velocity. The energy of each particle

$$E = \tfrac{1}{2}v^2 + V(x) = V(x) \tag{26}$$

depends on its position x. The corresponding energy distribution,

$$P(E) = 2\frac{|\psi_0|^2}{|dE/dx|} = \frac{2}{|dV/dx|}, \tag{27}$$

has poles at the equilibrium points where $dV/dx=0$. For the softcore Coulomb potential one finds

$$P(E) = \frac{2\epsilon V_0^2}{E^2\sqrt{V_0^2 - E^2}}, \quad V_0 = -\frac{Z}{\epsilon}. \tag{28}$$

The dominant contribution comes from the pole at $E=0$, corresponding to particles in high-lying Rydberg states with nearly zero initial energy. In practice the calculations are performed on a finite spatial interval, $|x|<x_b$, such that the maximum energy, $E=V(x_b)$, stays slightly below zero.

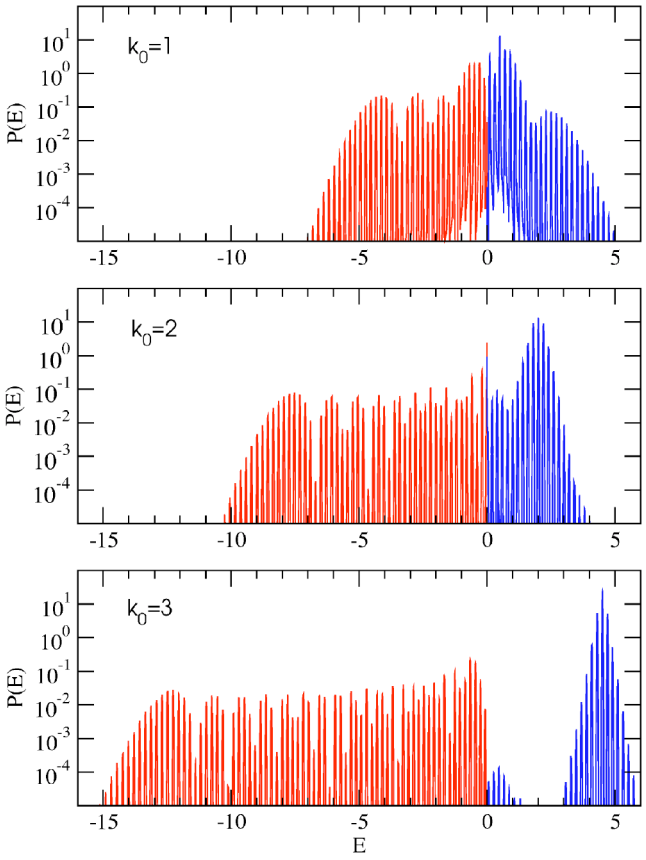

FIG. 6. Energy spectra for scattering with initial velocities $k_0 \geqslant 1$. With increasing velocities the spectrum becomes spatially asymmetric. The transmitted wave packet has an exponential energy distribution around the elastic peak. The reflected wave packet shows a plateau in a broad range of energies.

In the absence of preferred drift motion, the impact velocity of the electron is determined by the quiver motion in the laser field and by the attractive potential. The calculated energy spectrum is shown in Fig. 5. One actually can recognize the familiar ATI structure with a sequence of peaks separated by the photon energy. Higher photon orders form a scattering plateau extending up to the well-known ATI cutoff,

$$E_c = 10U_p = 2.5. \tag{29}$$

The figure shows both the spectrum on the left and on the right side of the scattering center being represented by negative and positive energies, respectively. There is nearly perfect spatial symmetry in this case.

We now discuss the scattering of Gaussian wave packets for a sequence of initial momenta. Increasing the initial momentum k_0, the spatial symmetry is broken and one observes completely different spectra for the transmitted and the reflected wave packets as shown in Fig. 6. On the right the scattering plateau disappears and instead an elastic peak with an exponential distribution of sidebands is observed. This corresponds to the fact that reflection into the right half space becomes strongly suppressed. It is only possible if an elec-

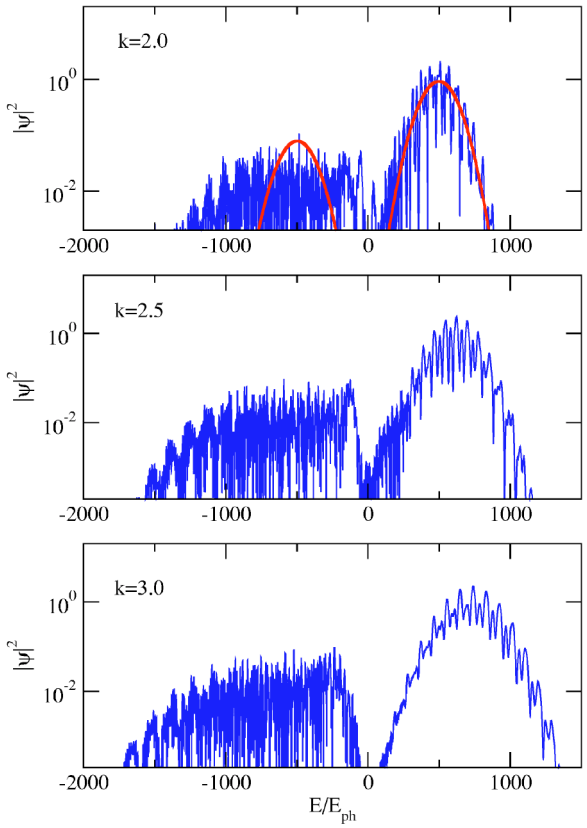

FIG. 7. Electron density distributions of the scattered wave function. For comparison the field-free solution is also indicated in the top panel.

tron, which has already been transmitted, is returned to the ion and then is rescattered again. In contrast, the incident electron can be directly reflected into the left half space leading to a plateau on this side. Due to the increased initial velocity the plateau gets strongly broadended and fast electrons far above the ATI cutoff (29) can be generated. The basic plateau features will be explained in terms of an instantaneous collision model in Sec. V.

The wave function of the final asymptotic state shows a corresponding asymmetry. In Fig. 7, we show the spatial distribution of the density $|\psi|^2$ at the final time for different initial velocities. At higher velocities, the transmitted wave packet preserves its Gaussian shape. One can recognize a periodic modulation of the Gaussian envelope that becomes quite regular for $k=3.0$. Classically, the laser field produces electron bunches by accelerating and decelerating electrons in subsequent half periods. The total bunch length is the distance $L_B=k_0T$ moved by the electron in a laser period T. Within each period one can expect two density maxima corresponding to the group of accelerated and decelerated particles. This explains the double-hump structure seen in Fig. 7. Quantum mechanically, the same effect can be described as an interference between the waves with the sideband energies $k_0^2/2\pm\omega_0$. The interference between these waves is modulated with the wave number $\Delta k=\Delta E/k=2\omega_0/k_0$, corresponding to a wavelength of one half bunch,

$$\lambda = 2\pi/\Delta k = k_0 T/2 = L_B/2. \tag{30}$$

Higher sidebands, being separated by $2n\omega_0$, produce harmonics but do not change the basic periodicity length. The shape of the reflected wave packet is more irregular, being a superposition of many waves in the plateau region.

V. INSTANTANEOUS COULOMB COLLISIONS

Electron-ion collisions in strong laser fields can be treated by the model of classical instantaneous collisions. Here we will derive the energy spectrum in this framework. First the model is considered in 1D for comparison with quantum calculations. Then 3D Coulomb collisions will be studied and an analytical expression for the energy distribution of the scattered particles will be derived.

Collisions in the laser field are called instantaneous if the duration of the collision is much shorter than the laser period. In the quantum approach, the de Broglie wave number of the momentum transfer, $\kappa=|k'-k|$, determines the characteristic interaction length $r=2\pi/\kappa$. If the impact velocity is of the order of the quiver velocity v_0, the criterion for instantaneous collisions can be expressed in the form

$$r/v_0 \ll T \Leftrightarrow \kappa\xi \gg 1, \tag{31}$$

where $T=2\pi/\omega_0$ denotes the laser period and $\xi=v_0/\omega_0$ the quiver amplitude. This condition is well satisfied for the present calculations with $\xi=5$ and $\kappa\gtrsim 1$.

For instantaneous elastic collisions at time t_c, the laser field can be taken as constant. From energy conservation, the momentum of the reflected particle is found to be

$$k + p_\varepsilon = -(k_0 + p_\varepsilon), \tag{32}$$

where $k_0>0$ denotes the drift momentum before and k after the collision and $p_\varepsilon=v_0\cos\phi$ the quiver momentum evaluated at the phase $\phi=\omega_0 t_c$. The new drift momentum $k=-(k_0+2p_\varepsilon)$ varies between the values

$$k_1 = -k_0 - 2v_0, \quad k_2 = -k_0 + 2v_0. \tag{33}$$

The electron will leave the field with an energy

$$E(\phi) = \tfrac{1}{2}[k_0 + 2p_\varepsilon(\phi)]^2 \tag{34}$$

that depends on the collision phase ϕ. Assuming that the collision phases are randomly distributed within the interval $[0,\pi]$ and that a fraction R of particles is reflected in each collision, the energy distribution can be obtained as

$$P(E) = \frac{R}{\pi}\frac{d\phi}{dE} = \frac{R}{\pi|k|\sqrt{(k-k_1)(k_2-k)}}, \tag{35}$$

where k is viewed as a function of $E=k^2/2$. Corresponding to the momenta $k_{1,2}$, the energy distribution has cutoffs at

$$E_{1,2} = \tfrac{1}{2}(k_0 \pm 2v_0)^2. \tag{36}$$

In Fig. 8, the model distribution (35) is compared with a calculated energy spectrum. The model gives an excellent approximation to the averaged quantum distribution with the proper cutoffs. The only unknown parameter in Eq. (35) is

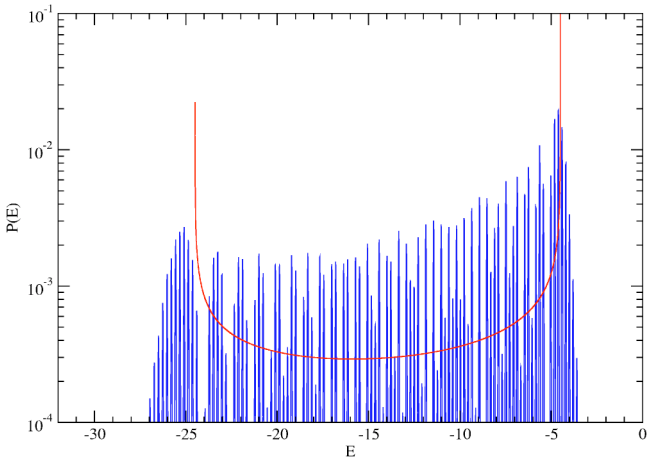

FIG. 8. Energy spectrum for $k_0=5$. Comparison of wave packet scattering with the instantaneous collision model. The average height of the plateau and its cutoffs are well reproduced by the model.

the reflection coefficient R. For most cases of interest, it can be gained with good accuracy from the field-free scattering problem.

The model of classical instantaneous collisions in a strong laser field can be generalized to 3D Coulomb collisions. We first briefly review the original work of Kroll and Watson, then compare the 3D rate of backscattered particles with the 1D model and finally derive the total angle-integrated energy distribution of the scattered particles in this framework. From the total energy distribution one can estimate the fraction of fast electrons that is produced in a plasma by large-angle electron-ion collisions.

For 3D Coulomb collisions, the momenta before and after the collision can be expressed as

$$\boldsymbol{p}_0 = \boldsymbol{k}_0 + \boldsymbol{p}_\varepsilon = p_0 \boldsymbol{n}_0, \quad \boldsymbol{p} = \boldsymbol{k} + \boldsymbol{p}_\varepsilon = p\boldsymbol{n}, \tag{37}$$

respectively, where $\boldsymbol{p}_\varepsilon = \boldsymbol{v}_0 \cos\phi$. At present, we restrict attention to parallel launch $\boldsymbol{k}_0 \| \boldsymbol{p}_\varepsilon$. The unit vector $\boldsymbol{n}_0$ is defined by the direction of $\boldsymbol{k}_0$. Then $k_0 > 0$ but p_0 may be positive or negative. For elastic collisions one has $p = p_0$ and the unit vector $\boldsymbol{n}$ is turned with respect to $\boldsymbol{n}_0$ by the scattering angle χ.

The energy transfer during the collision is defined as the difference of the asymptotic energies outside the laser field,

$$\Delta = \tfrac{1}{2}(k^2 - k_0^2). \tag{38}$$

Using Eq. (37), it can be expressed as

$$\Delta = \tfrac{1}{2}(\boldsymbol{p} + \boldsymbol{p}_0 - 2\boldsymbol{p}_\varepsilon)\cdot(\boldsymbol{p} - \boldsymbol{p}_0) = \tfrac{1}{2}(p^2 - p_0^2) - \boldsymbol{p}_\varepsilon \cdot (\boldsymbol{p} - \boldsymbol{p}_0). \tag{39}$$

Assuming elastic collisions, $p = p_0$, one obtains

$$\Delta = 2p_\varepsilon p_0 \sin^2(\chi/2), \tag{40}$$

where $p_0 = k_0 + p_\varepsilon$ and $p_\varepsilon = v_0 \cos\phi$. The energy transfer depends both on the collision phase ϕ and on the scattering angle χ. The dependence on ϕ is only implicit through the quiver momentum $p_\varepsilon(\phi)$. It is therefore sufficient to consider a half period, $0 < \phi < \pi$, where the quiver momentum assumes all its possible values between $-v_0$ and $+v_0$. The energy transfer Δ is a quadratic function of p_ε, which can be written in the normal form,

$$\Delta = \left[-\frac{k_0^2}{2} + 2\left(p_\varepsilon + \frac{k_0}{2}\right)^2 \right] \sin^2(\chi/2). \tag{41}$$

The energy transfer is zero for $p_\varepsilon = 0$ and $p_\varepsilon = -k_0$. It assumes its minimum value $-k_0^2/2$ for $p_\varepsilon = -k_0/2$ and $\chi = \pi$.

We now consider a uniform beam of electrons with density 1 and momentum p_0 being launched parallel to the electric field and scattered by an ion of charge Z for a given collision phase ϕ. The differential scattering rate into the solid angle $d\Omega = \sin\chi\, d\chi\, d\varphi$ and the collision phase interval $d\phi$ is by definition

$$dr = r(\chi,\phi) d\Omega\, d\phi, \quad r(\chi,\phi) = r_C[\chi, p_0(\phi)] w_\phi, \tag{42}$$

where $r_C(\chi, p_0) = |p_0|\ \sigma(\chi, p_0)$ is the Coulomb scattering rate with the Coulomb cross section,

$$\sigma(\chi, p_0) = \frac{Z^2}{4p_0^4 \sin^4(\chi/2)}, \tag{43}$$

and $w_\phi = 1/\pi$ denotes a constant probability distribution of the phase ϕ within the interval $[0, \pi]$. This is the well-known Kroll–Watson formula [Eq. (2.4) of Ref. 29] for potential scattering in a strong laser field.

Next, we wish to express the scattering rate as a function of the solid angle and the energy E of the scattered particles. This can be done by substituting ϕ by $E(\phi)$. As an intermediate step it is useful to express ϕ by $p_\varepsilon(\phi)$ yielding

$$dr = r(\chi, p_\varepsilon) d\Omega\, dp_\varepsilon, \quad r(\chi, p_\varepsilon) = r_C[\chi, p_0(p_\varepsilon)] w_{p_\varepsilon}, \tag{44}$$

where

$$w_{p_\varepsilon} = \frac{1}{\left|\dfrac{dp_\varepsilon}{d\phi}\right|} = \frac{1}{\pi\sqrt{v_0^2 - p_\varepsilon^2}} \tag{45}$$

denotes the probability distribution of quiver momentum. In the next step, the quiver momentum is substituted by the energy of the scattered particles using the relation

$$E(p_\varepsilon) = \tfrac{1}{2}k_0^2 + \Delta(p_\varepsilon). \tag{46}$$

The inverse of the function $\Delta(p_\varepsilon)$ is defined piecewise by

$$p_{\varepsilon,\sigma} = -\frac{k_0}{2} \pm \sqrt{\frac{\Delta}{2\sin^2(\chi/2)} + \frac{k_0^2}{4}}, \tag{47}$$

where $\sigma = \pm$ corresponds to the segments $p_\varepsilon \gtrless -k_0/2$, respectively. Using this notation, the scattering rate as a function of Ω and E assumes the form

$$dr = r(\chi, E) d\Omega\, dE, \quad r(\chi, E) = \sum_\sigma r_C(\chi, p_{0,\sigma}) w_{E,\sigma}, \tag{48}$$

with

$$\omega_{E,\sigma} = \frac{\omega_{p_{\varepsilon,\sigma}}}{\left|\frac{dE}{dp_{\varepsilon,\sigma}}\right|} = \frac{1}{2\pi \sin^2(\chi/2)|k_0 + 2p_{\varepsilon,\sigma}|\sqrt{v_0^2 - p_{\varepsilon,\sigma}^2}}. \tag{49}$$

This rate defines the energy distribution for a given scattering angle. It corrresponds to Eq. (2.7) of Ref. 29. Minor differences between the results are due to the phase dependence of the momentum transfer $\boldsymbol{Q}=\boldsymbol{p}-\boldsymbol{p}_0=p_0(\phi)(\boldsymbol{n}-\boldsymbol{n}_0)$, which apparently was not taken into account in the original work.[29]

For comparison with the 1D model, it is instructive to consider backscattering. Setting $\chi=\pi$, the scattering rate becomes

$$r(\pi,E) = \sum_\sigma \frac{r_C(\pi,p_{0,\sigma})}{\pi|k_\sigma|\sqrt{(k_\sigma - k_1)(k_2 - k_\sigma)}}, \tag{50}$$

where $k_{1,2}$ are given by Eq. (33) and $k_\sigma = \mp\sqrt{2E}$. This rate basically agrees with the 1D result (35). For simplicity, in the 1D case, only the branch with $k<0$ has been treated. Furthermore the Coulomb scattering rate $r_C(\pi,E)$ has to be replaced by a corresponding rate of reflected particles $\Gamma_0 R$ where Γ_0 defines the rate of incident particles and R the reflection coefficient in the 1D model.

After this brief summary, we now consider the problem of calculating the angle-integrated energy spectrum. The obvious way of integrating Eq. (48) over the solid angle does not appear very tractable analytically. To perform the integration, we therefore go back to the basic scattering rate (42), express the scattering angle by the energy transfer (40) for a given collision phase, and finally integrate over the range of collision phases. Performing the simple integration over the angle φ and substituting the scattering angle χ by Δ according to Eq. (40) yields

$$dr = r(\Delta,\phi)d\Delta\, d\phi, \quad r(\Delta,\phi) = \frac{2Z^2}{\Delta^2}\frac{|p_\varepsilon|}{p_0^2}. \tag{51}$$

The direction of the Δ integration is oriented along the positive axis for both positive and negative values of Δ. The integration variables Δ and ϕ are no longer independent of each other. For a given energy transfer, one has to take care of the allowable collision phases. The integration over collision phases with the proper integration limits is discussed in detail in the Appendix. The result is written in the general form

$$r(\Delta) = \frac{2Z^2}{\Delta^2}\Delta I(\Delta, v_0, k_0), \tag{52}$$

where $\Delta I(\Delta, v_0, k_0)$ is given by Eq. (A9).

As an example, for velocities $k_0 > 2v_0$, the integral assumes the explicit form

$$\Delta I = \frac{k_0\sqrt{v_0^2 - (p^+)^2}}{(k_0^2 - v_0^2)(k_0 + p^+)} - \frac{2v_0^2}{(k_0^2 - v_0^2)^{3/2}} \times \left[\arctan\left(\sqrt{\frac{(k_0 - v_0)(v_0 - p^+)}{(k_0 + v_0)(v_0 + p^+)}}\right) - \frac{\pi}{2}\Theta(-\Delta)\right], \tag{53}$$

where $\Theta(x)$ denotes the Θ function and

$$p^+ = -\frac{k_0}{2} + \sqrt{\frac{k_0^2}{4} + \frac{\Delta}{2}}$$

is the quiver momentum corresponding to backscattering ($\chi=\pi$) with the given energy Δ.

Finally, the energy spectrum is defined by the normalized scattering rate as

$$F(E) = \frac{r(\Delta)}{r_{\text{tot}}}, \tag{54}$$

with the total energy $E=\Delta+\frac{1}{2}k_0^2$ and the total scattering rate

$$r_{\text{tot}} = \int_{\Delta_{\min}}^{-\Delta_c} \frac{dr}{d\Delta}d\Delta + \int_{+\Delta_c}^{\Delta_{\max}} \frac{dr}{d\Delta}d\Delta.$$

The maximum and minimum energy transfers, $\Delta_{\max}$ and $\Delta_{\min}$, are given by Eq. (A6). A cutoff for small energy transfers, ΔE_c, is required to avoid the divergence of the Coulomb cross section in the binary collision model. This divergence can be removed by static or dynamic Debye screening in more complete many-particle theories. The energy cutoff is related to a maximum impact parameter $b_{\max}$ by

$$\Delta_c = 2p_\varepsilon p_0 \frac{b_\perp^2}{b_{\max}^2 + b_\perp^2}, \quad b_\perp = \frac{Z}{p_0^2}. \tag{55}$$

For the present purposes, we have chosen $b_{\max}=v_0/\omega_0 \gg b_\perp$ and have set $p_\varepsilon=v_0$ to estimate a lower bound

$$\Delta_c = \frac{2Z^2\omega_0^2}{v_0(k_0 + v_0)^3}. \tag{56}$$

In Fig. 9 the energy distribution (54) is shown for two different initial momenta $k_0=2$ and $k_0=3$ using the parameters $v_0=1$, $\omega_0=0.2$, and $Z=1$. One can recognize the scattering plateau in the energy range $(k_0-2v_0)^2/2 \leqslant E \leqslant (k_0+2v_0)^2/2$ and the elastic peak at the initial energy $E_0=k_0^2/2$. Note the descent of the scattering plateau. It results from the fact that smaller energy transfers can be reached within a wider range of scattering angles. One can now estimate the fraction of fast electrons produced at small impact parameters by the laser field. Integrating $F(E)$ over the high energy tail, the fraction of fast electrons with energies $E > E_0 + 3U_p$ is found to be 4×10^{-5} for $k_0=2$ and 1×10^{-5} for $k_0=5$. Of course, these numbers depend on the present choice of cutoff. However, since Eq. (56) is considered as a lower bound, it should lead to a conservative estimate of the fraction of fast electrons produced.

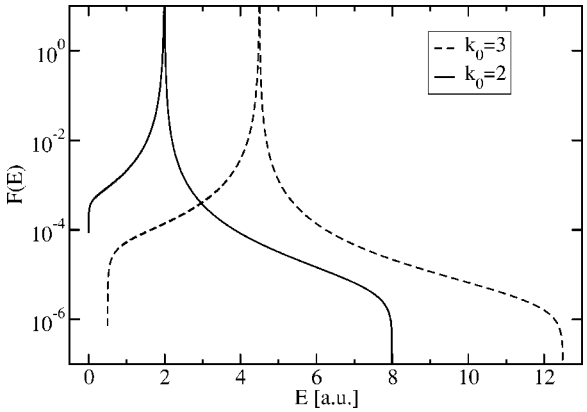

FIG. 9. Normalized energy spectra for classical instantaneous Coulomb collisions in a strong laser field. The electrons are launched parallel to the field with initial velocities $k_0=2$ and $k_0=3$. The quiver velocity is $v_0=1$. Depending on the scattering angle and the phase of the laser field, the scattered electrons can reach final energies within the range $(k_0-2v_0)^2/2 \leqslant E \leqslant (k_0+2v_0)^2/2$. The peaks in the distributions correspond to elastic scattering with the energy $E_0=k_0^2/2$.

VI. CONCLUSIONS

In this work, the energy distribution of electrons generated by electron-ion collisions in a strong laser field has been investigated. Particular attention has been devoted to the analysis of collisions with small impact parameters near and below an atomic unit, which are commonly omitted in plasma simulations. In such collisions a small but significant fraction of fast electrons can be produced by multiphoton scattering.

The energy distribution has been studied from the quantum-mechanical and the classical viewpoint. The quantum calculations are restricted to one dimension. They are similar to previous ATI studies, however, with the difference of using a smaller cutoff distance in the model potential and larger initial velocities of the incident electrons. With smaller cutoff distances, the quasiclassical behavior becomes violated and efficient reflection can be obtained in the 1D model. With increasing velocities, an asymmetry between transmitted and reflected electrons develops and at large velocities, the plateau of backscattered electrons can be completely separated from the exponential distribution of forward scattered electrons. Extending these methods to electrons scattered by ion pairs a characteristic double plateau in the energy distribution has been found recently.[33]

The classical analysis has been based on the model of instantaneous Coulomb collisions in the laser field. The instantaneous collision model can be compared with complete quantum calculations in 1D. It describes very well the limits and the average height of the energy plateau. In 3D the classical energy distribution has been analytically calculated and the fraction of fast electrons can be estimated from this distribution. This result may be useful for future short-pulse laser-plasma studies in the collisional regime. It will be interesting to include the fast electron distribution in plasma models where collisional ionization and recombination dynamics are important. More complete quantum treatments of electron-ion collisions might also be of interest to gain a better understanding of the applicability of the present classical approximation.

ACKNOWLEDGMENTS

This work was supported by the European Science Foundation (Strassbourg, France) through the scientific program FEMTO. One of the authors (H.-J.K.) is grateful for the hospitality received during his research visit at CELIA, Université Bordeaux 1.

APPENDIX: INTEGRAL OVER COLLISION PHASES

In this appendix, the integration of the scattering rate (51) over the collision phases will be performed. The basic integral is defined as

$$I=\int d\phi \frac{p_\varepsilon}{p_0^2}=v_0\int d\phi \frac{\cos\phi}{(k_0+v_0\cos\phi)^2}. \tag{A1}$$

The result of the integration can be expressed up to an arbitrary constant as

$$I=\frac{k_0 v_0 \sin\phi}{(k_0^2-v_0^2)(k_0+v_0\cos\phi)}-\frac{v_0^2}{k_0^2-v_0^2}J,$$
$$J=\begin{cases}\dfrac{2}{\sqrt{k_0^2-v_0^2}}\arctan x & \text{for } k_0>v_0\\ \dfrac{1}{\sqrt{v_0^2-k_0^2}}\ln\left|\dfrac{x+1}{x-1}\right| & \text{for } k_0<v_0,\end{cases} \tag{A2}$$
$$x=\frac{|k_0-v_0|}{|k_0^2-v_0^2|^{3/2}}\tan(\phi/2),$$

where $k_0>0$ and $v_0>0$ are positive. It is convenient to substitute the phase ϕ by the quiver momentum p_ε by use of the relations

$$v_0\cos\phi=p_\varepsilon,$$
$$v_0\sin\phi=\sqrt{v_0^2-p_\varepsilon^2}, \tag{A3}$$
$$\tan\frac{\phi}{2}=\sqrt{\frac{v_0-p_\varepsilon}{v_0+p_\varepsilon}}.$$

Setting $I=I^>$ for $k_0>v_0$ and $I=I^<$ for $k_0<v_0$, one obtains

$$I^>(p_\varepsilon)=\frac{k_0\sqrt{v_0^2-p_\varepsilon^2}}{(k_0^2-v_0^2)(k_0+p_\varepsilon)}-\frac{2v_0^2}{(\sqrt{k_0^2-v_0^2})^3}\arctan x,$$
$$I^<(p_\varepsilon)=\frac{v_0^2}{(\sqrt{v_0^2-k_0^2})^3}\ln\left|\frac{1+x}{1-x}\right|-\frac{k_0\sqrt{v_0^2-p_\varepsilon^2}}{(v_0^2-k_0^2)(k_0+p_\varepsilon)}, \tag{A4}$$

with

$$x=\sqrt{\frac{|k_0-v_0|}{k_0+v_0}\,\frac{v_0-p_\varepsilon}{v_0+p_\varepsilon}}.$$

We now discuss the proper integration limits for a given energy transfer. The original integration variables are the scattering angle χ and the collision phase ϕ. The integration

domain is the square $0 \leqslant \chi \leqslant \pi$, $0 \leqslant \phi \leqslant \pi$. Changing to the variables Δ and p_ε by use of Eqs. (40) and (A3), the integration domain is mapped to

$$\begin{aligned} &v_0 \geqslant p_\varepsilon \geqslant 0 \quad \text{for } p_\varepsilon > 0, \\ &-v_0 \leqslant p_\varepsilon \leqslant 0 \quad \text{for } p_\varepsilon < 0, \\ &0 \leqslant \Delta \leqslant \eta(p_\varepsilon) \quad \text{for } \Delta > 0, \\ &\eta(p_\varepsilon) \leqslant \Delta \leqslant 0 \quad \text{for } \Delta < 0, \end{aligned} \tag{A5}$$

where

$$\eta(p_\varepsilon) = 2p_0 p_\varepsilon = \tfrac{1}{2}(k_0 + 2p_\varepsilon)^2 - \tfrac{1}{2}k_0^2$$

is the energy transfer for backscattering with $\chi = \pi$. For $p_\varepsilon < 0$, the integration limits in Eq. (A5) have been reversed such that the magnitude of p_ε in the integrand of Eq. (51) can be dropped.

The quadratic function $\eta(p_\varepsilon)$ has a minimum $-k_0^2/2$ at $p_\varepsilon = -k_0/2$. It corresponds to the total loss of the energy of the incident particle. At this point, the final momentum $k = -k_0 - 2p_\varepsilon$ of the backscattered particle changes its sign. The zeroes of $\eta(p_\varepsilon)$ are at $p_\varepsilon = 0$ and $p_\varepsilon = -k_0$. The energy transfer is positive for $p_\varepsilon > 0$ or $p_\varepsilon < -k_0$ and negative for $-k_0 < p_\varepsilon < 0$. The maximum and minimum energy transfers in the interval $-v_0 < p_\varepsilon < v_0$ are given by

$$\begin{aligned} \Delta_{\max} &= \frac{k_1^2}{2} - \frac{k_0^2}{2}, \\ \Delta_{\min} &= \frac{k_2^2}{2}\Theta(-k_2) - \frac{k_0^2}{2}, \end{aligned} \tag{A6}$$

where $k_{1,2} = -k_0 \mp 2v_0$. The maximum value is the boundary value $\eta(+v_0)$. Depending on the sign of k_2, the minimum value is either the boundary value $\eta(-v_0)$ or the absolute minimum $\eta(-k_0/2)$.

To obtain the energy distribution the integration over the collision phases has to be carried out for a fixed value of Δ within $\Delta_{\min} \leqslant \Delta \leqslant \Delta_{\max}$. The integration limits are determined by the zeroes of $\eta(p_\varepsilon) - \Delta = 0$, which are given by

$$p^{\pm} = -\frac{k_0}{2} \pm \frac{1}{2}\sqrt{k_0^2 + 2\Delta}. \tag{A7}$$

The integration domain on the p_ε axis can be subdivided into three intervals,

$$\begin{aligned} &D_1 = [v_0, p^+] \quad \text{for } \Delta > 0, \\ &D_2 = [p^>, p^+] \quad \text{for } \Delta < 0, \\ &D_3 = [p^<, p^-] \quad \text{for } \Delta > 0, \end{aligned}$$

where

$$p^> = \max\{-v_0, p^-\}, \quad p^< = \min\{-v_0, p^-\}.$$

Evaluating the integral (A1) for each interval and adding the contributions yields

$$\begin{aligned} \Delta I = \Theta(\Delta)\{I(p^+) - I(v_0) + I(p^-) - I(p^<)\} + \Theta(-\Delta)\{I(p^+) \\ - I(p^>)\}. \end{aligned} \tag{A8}$$

It is noted that

$$I(v_0) = 0, \quad I(-v_0) = -\frac{2v_0^2}{(k_0^2 - v_0^2)^{3/2}}\frac{\pi}{2}\Theta(k_0 - v_0).$$

Depending on the parameters v_0, k_0, and Δ, one can distinguish three cases with

$$\Delta I = \begin{cases} I^>(p^+) - \Theta(-\Delta) I^>(-v_0) & \text{for } -k_0 < p^- < -v_0 \\ I^>(p^+) - \Theta(-\Delta) I^>(p^-) & \text{for } -k_0 < -v_0 < p^- \\ I^<(p^+) - \{\Theta(-\Delta) - \Theta(\Delta)\} I^<(p^-) & \text{for } -v_0 < p^- < -k_0. \end{cases} \tag{A9}$$

Here $I^>(p_\varepsilon)$ and $I^<(p_\varepsilon)$ are given by Eq. (A4). This is the final result to be used in the scattering rate (52).

[1] B. Yang, K. J. Schafer, B. Walker, K. C. Kulander, P. Agostini, and L. F. DiMauro, Phys. Rev. Lett. **71**, 3770 (1993).
[2] G. G. Paulus, W. Nicklich, H. Xu, P. Lambropoulos, and H. Walther, Phys. Rev. Lett. **72**, 2851 (1994).
[3] M. Lewenstein, K. C. Kulander, K. J. Schafer, and P. H. Bucksbaum, Phys. Rev. A **51**, 1495 (1995).
[4] A. Lohr, M. Kleber, and R. Kopold, Phys. Rev. A **55**, R4003 (1997).
[5] S. P. Goreslavskii and S. V. Popruzhenko, JETP **90**, 778 (2000).
[6] R. Kopold, D. B. Milošević, and W. Becker, Phys. Rev. Lett. **84**, 3831 (2000).
[7] V. P. Silin, Sov. Phys. JETP **20**, 1510 (1965).
[8] C. D. Decker, W. B. Mori, J. M. Dawson, and T. Katsouleas, Phys. Plasmas **1**, 4043 (1994).
[9] G. M. Fraiman, V. A. Mironov, and A. A. Balakin, Phys. Rev. Lett. **82**, 319 (1999).
[10] G. M. Fraiman, V. A. Mironov, and A. A. Balakin, JETP **88**, 254 (1999).
[11] G. M. Fraiman, A. A. Balakin, and V. A. Mironov, Phys. Plasmas **8**, 2502 (2001).
[12] T. Bornath, M. Schlanges, P. Hilse, and D. Kremp, Phys. Rev. E **64**, 026414 (2001).
[13] H.-J. Kull and L. Plagne, Phys. Plasmas **8**, 5244 (2001).
[14] A. Brantov, W. Rozmus, R. Sydora, C. E. Capjack, V. Y. Bychenkov, and V. T. Tikhonchuk, Phys. Plasmas **10**, 3385 (2003).
[15] R. C. Issac, G. Vieux, B. Ersfeld, E. Brunetti, S. P. Jamison, J. Gallacher, D. Clark, and D. A. Jaroszynski, Phys. Plasmas **11**, 3491 (2004).
[16] G. G. Paulus, F. Lindner, H. Walther, A. Baltuška, E. Goulielmakis, M. Lezius, and F. Krausz, Phys. Rev. Lett. **91**, 253004 (2003).
[17] J. Javanainen, J. H. Eberly, and Q. Su, Phys. Rev. A **38**, 3430 (1988).
[18] J. Javanainen and J. Eberly, Phys. Rev. A **39**, 458 (1989).
[19] K. Boucke, H. Schmitz, and H.-J. Kull, Phys. Rev. A **56**, 763 (1997).

[20]L. Roso-Franco and J. H. Eberly, J. Opt. Soc. Am. B **7**, 407 (1990).
[21]W. G. Greenwood and J. H. Eberly, Phys. Rev. A **43**, 525 (1991).
[22]R. Grobe, D. G. Lappas, and J. H. Eberly, Phys. Rev. A **43**, 388 (1991).
[23]R. Grobe and J. H. Eberly, Phys. Rev. A **47**, 719 (1993).
[24]Q. Su, J. H. Eberly, and J. Javanainen, Phys. Rev. Lett. **64**, 862 (1990).
[25]Q. Su and J. H. Eberly, J. Opt. Soc. Am. B **7**, 564 (1990).
[26]H.-J. Kull, J. Görlinger, and L. Plagne, Laser Phys. **10**, 151 (2000).
[27]N. L. Manakov, A. F. Starace, A. V. Flegel, and M. V. Frolov, JETP Lett. **76**, 258 (2002).
[28]F. V. Bunkin and M. V. Fedorov, Sov. Phys. JETP **22**, 844 (1966).
[29]N. M. Kroll and K. M. Watson, Phys. Rev. A **8**, 804 (1973).
[30]F. B. Bunkin, A. E. Kazakov, and M. V. Fedorov, Sov. Phys. Usp. **15**, 416 (1973).
[31]J. Crank and P. Nicholson, Proc. Cambridge Philos. Soc. **43**, 50 (1947).
[32]A. Goldberg, H. M. Schey, and J. L. Schwartz, Am. J. Phys. **35**, 177 (1967).
[33]J. Görlinger, H.-J. Kull, and V. T. Tikonchuk, Laser Phys. **15**, 245 (2005).